Mass and metallicity scaling relations of high-redshift star-forming galaxies selected by GRBs

M. Arabsalmani,[1,2,3,4]★ P. Møller,[3] D. A. Perley,[4,5] W. Freudling,[3] J. P. U. Fynbo,[4]
E. Le Floc'h,[1] M. A. Zwaan,[3] S. Schulze,[6,7] N. R. Tanvir,[8] L. Christensen,[4]
A. J. Levan,[9] P. Jakobsson,[10] D. Malesani,[4] Z. Cano,[11] S. Covino,[12] V. D'Elia,[13,14]
P. Goldoni,[15] A. Gomboc,[16] K. E. Heintz,[4] M. Sparre,[4,17] A. de Ugarte Postigo[4,10]
and S. D. Vergani[2]

[1]*CEA/DSM/IRFU, CNRS, Université Paris-Diderot, F-91190 Gif, France*
[2]*GEPI, Observatoire de Paris, PSL Research University, CNRS, Place Jules Janssen, F-92190 Meudon, France*
[3]*European Southern Observatory, Karl-Schwarzschild-Strasse 2, D-85748 Garching bei München, Germany*
[4]*Dark Cosmology Centre, Niels Bohr Institute, University of Copenhagen, Juliane Maries Vej 30, DK-2100 Copenhagen Ø, Denmark*
[5]*Astrophysics Research Institute, Liverpool John Moores University, IC2, Liverpool Science Park, 146 Brownlow Hill, Liverpool L3 5RF, UK*
[6]*Instituto de Astrofísica, Pontificia Universidad Católica de Chile, Vicũna Mackenna 4860, 7820436 Macul, Santiago, Chile*
[7]*Millennium Institute of Astrophysics, Vicũna Mackenna 4860, 7820436 Macul, Santiago, Chile*
[8]*Department of Physics and Astronomy, University of Leicester, University Road, Leicester LE1 7RH, UK*
[9]*Department of Physics, University of Warwick, Coventry CV4 7AL, UK*
[10]*Centre for Astrophysics and Cosmology, Science Institute, University of Iceland, Dunhagi 5, 107 Reykjavik, Iceland*
[11]*Instituto de Astrofísica de Andalucía (IAA-CSIC), Glorieta de la Astronomía s/n, E-18008 Granada, Spain*
[12]*INAF – Osservatorio Astronomico di Brera, Via E. Bianchi 46, I-23807 Merate (LC), Italy*
[13]*INAF – Osservatorio Astronomico di Roma, Via Frascati 33, I-00040 Monteporzio Catone, Italy*
[14]*ASI-Science Data Centre, Via del Politecnico snc, I-00133 Rome, Italy*
[15]*APC, Astroparticule et Cosmologie, Universite Paris Diderot, CNRS/IN2P3, CEA/Irfu, Observatoire de Paris, Sorbonne Paris CitÉ, 10 Rue Alice Domon et LÉonie Duquet, F-75205 Paris Cedex 13, France*
[16]*School of Science, University of Nova Gorica, Vipavska 11c, 5270 Ajdovščina, Slovenia*
[17]*Heidelberger Institut für Theoretische Studien, Schloss-Wolfsbrunnenweg 35, D-69118 Heidelberg, Germany*

ABSTRACT

We present a comprehensive study of the relations between gas kinematics, metallicity and stellar mass in a sample of 82 gamma-ray burst (GRB)-selected galaxies using absorption and emission methods. We find the velocity widths of both emission and absorption profiles to be a proxy of stellar mass. We also investigate the velocity–metallicity correlation and its evolution with redshift. Using 33 GRB hosts with measured stellar mass and metallicity, we study the mass–metallicity relation for GRB host galaxies in a stellar mass range of $10^{8.2}$–$10^{11.1}$ $M_\odot$ and a redshift range of $z \sim 0.3$–3.4. The GRB-selected galaxies appear to track the mass–metallicity relation of star-forming galaxies but with an offset of 0.15 towards lower metallicities. This offset is comparable with the average error bar on the metallicity measurements of the GRB sample and also the scatter on the mass–metallicity relation of the general population. It is hard to decide whether this relatively small offset is due to systematic effects or the intrinsic nature of GRB hosts. We also investigate the possibility of using absorption-line metallicity measurements of GRB hosts to study the mass–metallicity relation at high redshifts. Our analysis shows that the metallicity measurements from absorption methods can significantly differ from emission metallicities and assuming identical measurements from the two methods may result in erroneous conclusions.

Key words: gamma-ray burst: general – galaxies: evolution – galaxies: high-redshift – galaxies: ISM – galaxies: kinematics and dynamics – galaxies: star formation.

★ E-mail: maryam.arabsalmani@cea.fr

1 INTRODUCTION

Long-duration gamma ray bursts (GRBs) are beacons of star-forming galaxies (Sokolov et al. 2001; Le Floc'h et al. 2003; Christensen, Hjorth & Gorosabel 2004; Fruchter et al. 2006) up to very high redshifts (the highest confirmed spectroscopic redshift for a GRB is $z = 8.2$; Salvaterra et al. 2009; Tanvir et al. 2009). The detectability of these extremely bright and dust-penetrating explosions is independent of the brightness and dust content of their host galaxies. Hence they provide a unique method for sampling star-forming galaxies throughout the Universe without a luminosity bias, something that significantly impacts even the deepest flux-limited galaxy surveys.

The presence of GRB afterglows makes it possible to study their host galaxies through the absorption features that their interstellar media (ISM) imprint on the GRBs spectra (see e.g. Castro et al. 2003; Vreeswijk et al. 2004; Chen et al. 2005; Watson et al. 2006; Fynbo et al. 2009; de Ugarte Postigo et al. 2012) up to the highest redshifts (Sparre et al. 2014; Hartoog et al. 2015). The fact that GRBs fade away allow emission studies of their hosts without interference of the bright GRBs (for emission studied of GRB hosts see e.g. Savaglio, Glazebrook & Le Borgne 2009; Castro Cerón et al. 2010; Krühler et al. 2015; Perley et al. 2016b). This is not the case for other absorbing systems such as those in the sightlines of quasars where even at low redshifts detecting the galaxy counterparts has proven to be extremely challenging due to the presence of the bright background quasars (Warren et al. 2001; Christensen et al. 2014). Independent measurements of galaxy properties (such as metallicity and gas kinematics) using both absorption and emission methods and their connection with stellar mass can provide insight into galaxy formation and evolution. GRBs provide an opportunity for performing such studies for a population of star-forming galaxies.

Absorption-line studies of GRB host galaxies have led to accurate measurements of abundances, metallicity, dust and kinematics up to redshifts $z \sim 6.0$ (e.g. Prochaska et al. 2008; Fynbo et al. 2009; Zafar et al. 2011; Thöne et al. 2013; Arabsalmani et al. 2015a; Cucchiara et al. 2015). Emission-line studies have provided stellar masses, star formation rates, kinematics and emission-line metallicity measurements (e.g. Savaglio et al. 2009; Castro Cerón et al. 2010; Krühler et al. 2015), though limited to redshifts $\lesssim 3.0$ due to the sensitivity limits of currently available telescopes [also at $z \gtrsim 3$ the key diagnostic lines for emission-line metallicity measurements are redshifted out of the near-infrared (NIR) bands]. However, the connection between the information inferred from the two methods is yet to be studied. Metallicity measurements and kinematics are two properties that are independently inferred from both methods, using metal absorption profiles and bright nebular emission lines, respectively. These profiles trace different regimes and gas phases in galaxies. As a result, the two sets of line profiles typically have different kinematic signatures (e.g. Castro-Tirado et al. 2010). Also, metallicity measurements from absorption and emission methods not only trace the metal enrichment of gas in different regions of galaxies, but also are based on totally different diagnostics (see Friis et al. 2015).

It is of much interest to investigate whether GRB host galaxies sample the general star-forming galaxy population, or if they represent a distinct galaxy population. This question has been the core of many studies in the research field of GRB hosts (see Fynbo et al. 2008; Savaglio et al. 2009; Arabsalmani et al. 2015a; Greiner et al. 2015; Schulze et al. 2015; Perley et al. 2016b, as a few examples for addressing this question). Any systematic differences between GRB hosts and the average field galaxy population provide important clues as to the conditions required to produce GRBs, and underpin attempts to use GRBs to probe galaxy evolution. To date many works have indicated that GRB production is disfavoured in high-metallicity environments (e.g. Wolf & Podsiadlowski 2007; Modjaz et al. 2008; Savaglio et al. 2009; Graham & Fruchter 2013; Vergani et al. 2015; Perley et al. 2016b), but it is less clear whether other factors are also relevant as some GRBs have been associated with metal-rich galaxies (e.g. Krühler et al. 2012; Savaglio et al. 2012). A potentially powerful diagnostic is the mass–metallicity (MZ) relation, which has frequently been discussed for GRB hosts (Savaglio, Glazebrook & Le Borgne 2006; Stanek et al. 2006; Kewley et al. 2007; Nuza et al. 2007; Han et al. 2010; Levesque et al. 2010; Mannucci, Salvaterra & Campisi 2011; Graham & Fruchter 2013; Japelj et al. 2016; Vergani et al. 2017), since it effectively allows us to investigate whether at a given metallicity/redshift the hosts have typical masses. However, the consistency of GRB host galaxies with the MZ relation of the general star-forming galaxy population has been a subject under debate.

In this paper we use a large sample of GRB host galaxies with measured properties from absorption and emission methods in order to combine our understanding of this galaxy population from the two methods. We study the scaling relations between gas kinematics, metallicity and stellar mass and investigate their redshift evolution. Our sample and the methods used to measure the galaxy properties are described in Section 2. In Section 3 we compare the kinematic characteristics of gas in both emission and absorption, and investigate the connection between them and the stellar mass. The relationships between gas kinematics and metallicity in both absorption and emission are discussed in Section 4. Finally, we present the MZ relation for our large GRB host sample in Section 5 and compare it with that of the general population of star-forming galaxies. We discuss the possibility of using absorption metallicity measurements to study the MZ relation in Section 6. Our results are summarized in Section 7.

2 SAMPLE AND MEASUREMENTS

2.1 Sample

Our main goal is to investigate the scaling relations between the gas kinematics and metallicity, inferred from both absorption and emission methods, and stellar mass for GRB host galaxies. In total we are then considering five parameters describing five properties: absorption and emission metallicities, absorption and emission velocity widths and stellar mass. Currently all five parameters are known for only a single galaxy (host of GRB 121024A), and we therefore compile (mainly from the literature) a sample containing GRB hosts for which at minimum two of the considered parameters are available. This allows us to construct subsamples to study relations in any projection of the 5D parameter space. In order to have a sample with consistently determined parameters we use the sample of Krühler et al. (2015) for all the emission-line metallicity and emission-line velocity width measurements. Also all the stellar mass measurements are taken from Krühler & Schady (2017). We take the absorption-line metallicities from various sources in the literature. Absorption-line velocity width measurements are either presented in this work using the Very Large Telescope (VLT)/X-shooter GRB afterglow sample (the description of the data is presented in Selsing et al., in preparation) or taken from Arabsalmani et al. (2015a).

Table 1. GRB host sample (82 GRB hosts) with GRB name and redshift in first and second columns (see the online version of the paper for the complete table with all values and the corresponding references listed). All stellar masses are taken from Krühler & Schady (2017). All emission-line metallicities and emission-line velocity widths are taken from Krühler et al. (2015). Absorption-line velocity widths are from Arabsalmani et al. (2015a) and this work. Absorption-line metallicities are from Savaglio (2006), Ledoux et al. (2009), Fynbo et al. (2006), Price et al. (2007), De Cia et al. (2011), D'Elia et al. (2010, 2011, 2014), Thöne et al. (2013), Savaglio et al. (2012), Sparre et al. (2014), Krühler et al. (2013), Cucchiara et al. (2015) and Friis et al. (2015).

GRB	z	GRB	z	GRB	z
000926A	2.0379	080210A	2.641	110918A	0.984
050416A	0.654	080413B	1.101	111008A	5.0
050730A	3.969	080602A	1.820	111123A[b]	3.1513
050820A	2.6147	080605A	1.641	111209A	0.677
050824A	0.828	080805A	1.505	111211A	0.479
050915A[a]	2.528	081008A	1.968	111228A[a]	0.715
050922C	2.199	081109A	0.979	120118B[a]	2.9428
051016B	0.936	081210A[a]	2.063	120119A	1.729
051022A	0.806	081221A	2.259	120327A	2.815
051117B	0.481	090113A	1.749	120422A	0.283
060204B	2.339	090313A	3.374	120624B	2.197
060206A	4.048	090323A[b]	3.583	120714B	0.399
060306A	1.560	090407A	1.448	120722A	0.959
060510B	4.941	090926A	2.107	120815A	2.358
060604A	2.1355	090926B	1.243	120909A	3.9293
060719A	1.532	091018A	0.971	121024A	2.301
060729A	0.543	091127A	0.490	130408A	3.757
060814A	1.922	100219A	4.667	130427A	0.340
061021A	0.345	100418A	0.624	130925A	0.348
061110A[a]	0.758	100424A[a]	2.4656	131103A	0.596
061202A	2.254	100508A	0.520	131105A	1.6854
070306A	1.497	100606A	1.5545	131231A	0.643
070318A	0.840	100615A	1.3978	140213A	1.19
070328A[a]	2.063	100621A	0.543	140301A	1.4155
070521A	2.087	100814A	1.439	140430A	1.6019
071021A	2.452	100816A	0.805	140506A	0.889
071031A	2.692	110808A	1.3490		
080207A	2.086	110818A[a]	3.361		

[a]For these hosts the emission velocity width is measured from H β line instead of H α line.
[b]For these hosts the emission velocity width is measured from [O III] line instead of H α line.

We do not apply any selection criteria based on the properties of GRBs themselves as such selection methods do not necessarily imply well-defined selection criteria on properties of the hosts. We therefore include the host galaxies of dust-obscured and/or dark GRBs (GRBs with significant dust attenuation and/or $\beta_{OX} \gtrsim 0.5$; see Jakobsson et al. 2004; Greiner et al. 2011; Perley et al. 2013) in our sample. This allows us to sample the largest possible range in the 5D parameter space that is critical in studying the scaling relations of GRB host population. The two ultralong GRBs, GRB 111209A (Levan et al. 2014) and GRB 130925A (Schady et al. 2015), are as well included in our sample.

The full sample of 82 GRB host galaxies is listed in Table 1 (see the online version of this paper for the complete table with all values listed). The relevant subsamples count 52 GRB host galaxies with stellar masses and emission-line velocity widths, 43 with emission-line metallicities and emission-line velocity widths, 33 with stellar masses and emission-line metallicities, seven with stellar masses and absorption-line velocity widths, 19 with absorption-line metallicities and absorption-line velocity widths, three with stellar masses and absorption-line metallicities, 10 with emission-line and absorption-line velocity widths and one GRB host with emission-line and absorption-line metallicity measurements.

2.2 Measurements

GRB host galaxies display very high column densities of neutral hydrogen, typically several times larger than the damped Lyman α (DLA) threshold (see e.g. Jakobsson et al. 2006; Fynbo et al. 2009). In systems with such high H I column densities the low-ion profiles trace the neutral hydrogen and hence the kinematic characteristics of these profile represent those of the neutral gas. The absorption profiles in GRBs spectra usually show several components or clouds tracing the velocity field in their host galaxies, similar to those of the DLA systems in the spectra of quasars. Each of these clouds has a broadening of a few km s^{-1} (see e.g. Dessauges-Zavadsky et al. 2006), but the total velocity width of the system is much larger, varying from a few tens of km s^{-1} to several hundreds of km s^{-1}. These absorption profiles trace only the gas in a narrow beam along the GRB sightline and therefore the velocity width of these lines provide the averaged velocity over the regions along the GRB sightline only.

To measure the velocity width of the neutral gas from low-ion absorption profiles, we use Δv_{90} as defined in Prochaska & Wolfe (1998), which is the velocity interval that contains 90 per cent of the area under the apparent optical depth spectrum (see Fig. A1 for an example). In order to measure Δv_{90} one needs to carefully choose the metal lines that are suitable for such measurement. Such a line should neither be weak nor saturated, as these would lead to under- and over-estimation of the velocity width, respectively (Ledoux et al. 2006; Møller et al. 2013). Thus, we need to identify at least one low-ion metal profile in the GRB spectrum that is suitable for measuring the line width. Identifying such a line for measuring the velocity width can be hard if the signal-to-noise ratio (S/N) of the spectrum is not high enough. In addition to this, we need to take care of the smearing effect caused by the resolution of the spectrograph. For this we use the method discussed by Arabsalmani et al. (2015a) and compute the intrinsic velocity width from

$$\Delta v_{90} = \left[\Delta v_{90,\text{meas}}^2 - (1.4 \times \text{FWHM})^2 \right]^{0.5}, \tag{1}$$

where $\Delta v_{90,\text{meas}}$ is the measured value of the velocity width and FWHM is the corresponding full width at half-maximum of the instrument resolution. The X-shooter spectrograph (Vernet et al. 2011) consists of three separate spectrographs covering the spectral regions from the atmospheric cut-off to 550 nm (UVB), from 550 to 1000 nm (VIS) and from 1000 nm to the K band (NIR). The spectral resolution is in the range 4000–17000 depending on the arm, the slit and/or the seeing during the observations. For the observations used in this study the FWHM of spectroscopic resolution was typically in the range 30–60 km s^{-1}. We use the r parameter (introduced in Arabsalmani et al. 2015a),

$$r := \frac{\Delta v_{90,\text{meas}} - \Delta v_{90}}{\Delta v_{90}}, \tag{2}$$

and choose a conservative approach of only considering systems correctable if $r \leq 0.4$. We have X-shooter optical spectra with sufficient S/N for 12 GRBs in order to measure Δv_{90} (see Table 2). The smearing effect of the instrument resolution does not allow Δv_{90} measurements for two of them (see the values of parameter r in column 5 of Table 2).

For gas seen in emission, we take all the H α velocity dispersion ($\sigma_{H\alpha}$) and the emission-line metallicity measurements from

Table 2. Measurements for velocity width of absorption lines (Δv_{90}). Columns 1–5 are GRB name, redshift, Δv_{90}, the absorption profile used for Δv_{90} measurement and the smearing correction factor as defined in equation (2).

GRB	Redshift	Δv_{90} (km s^{-1})	Low-ion line	r
091018A	0.971	146	Si II, 1808	0.15
100418A	0.62	181	Mn II, 2576	0.10
100814A	1.439	211	Fe II, 2600	0.03
111209A	0.677	187	Fe II, 2374	0.10
111211A	0.4786	98	Mn II, 2594	0.31
111228A	0.7164	30	Mn II, 2594	1.90
120909A	3.9293	145	Ni II, 1370	0.06
121024A	2.301	437	Mn II, 2594	0.01
130408A	3.757	97	Si II, 1808	0.13
130427A	0.340	60	Mn II, 2576	0.72
131231A	0.643	143	Fe II, 2374	0.16
140213A	1.19	151	Fe II, 2382	0.14

Krühler et al. (2015) where they use VLT/X-Shooter observations of the host galaxies and base their metallicity measurements on calibrators from Nagao, Maiolino & Marconi (2006) and Maiolino et al. (2008). Stellar mass measurements are all taken from Krühler & Schady (2017) where the measurements are based on modelling the spectral energy distributions (SEDs) of the host galaxies with LEPHARE (Arnouts et al. 1999; Ilbert et al. 2006), with galaxy templates from Bruzual & Charlot (2003), assuming exponentially declining star formation histories with the dust attenuation curve from Calzetti et al. (2000), and Chabrier initial mass function (IMF; Chabrier 2003).

3 VELOCITY WIDTH AS A PROXY OF STELLAR MASS

The relation between gas kinematics and luminosity was first introduced for nearby disc galaxies through the Tully–Fisher (TF) relation (Tully & Fisher 1977, using the inferred rotational velocity from the H I 21 cm emission line width). This was later extended to higher redshifts using optical lines, and to the relation between stellar mass

and rotational velocity known as the stellar mass Tully–Fisher (sTF) relation (see Kassin et al. 2007, for sTF at $0.1 < z < 1.2$). Initial investigations of high-redshift galaxies found no correlation (Vogt et al. 1996; Simard & Pritchet 1998), hinting to anomalous kinematics of high-redshift galaxies. This was confirmed by studies of Lyman-break galaxies at $z \sim 3$ (Pettini et al. 1998, 2001) and by UV-selected galaxies at $z \sim 2$ (Erb et al. 2006), from the integrated velocity width of nebular emission lines. However, recent studies (especially with the help of resolved 2D kinematics) show that the sTF relation holds for high-redshift galaxies, albeit with larger scatter compared to the local population (Puech et al. 2008, 2010; Miller et al. 2011; Glazebrook 2013; Christensen & Hjorth 2017).

We have stellar mass and $\sigma_{H\alpha}$ measurements for 52 GRB hosts in our sample, covering a redshift range from $z = 0.28$ to 3.58. The 52 hosts are presented in the left-hand panel of Fig. 1. We clearly see a correlation between stellar mass and $\sigma_{H\alpha}$ (see also Christensen & Hjorth 2017). The velocity width of the H α emission line contains contributions from rotational velocity. But one should be careful not to erroneously interpret this width as an upper limit to the rotational velocity of the ionized gas in the galaxy. The full rotational velocity will only appear in the broadening of the H α line if the observations are deep enough to pick up faint emission from the full extent of the ionized gas in the star-forming disc. Therefore we do not consider the M_*–$\sigma_{H\alpha}$ relation, shown in Fig. 1, as a sTF relation. However, the existence of such a correlation for the GRB host sample with its large redshift range is interesting in light of the sTF relation. We also emphasize that the velocity width of the H α line should not be confused with the equivalent width of the H α line. The latter measures the ratio of H α flux, and hence star formation rate (SFR; Kennicutt & Evans 2012), to the stellar continuum. The H α equivalent width thus provides a proxy for specific SFR (Fumagalli et al. 2012). Whereas the H α velocity width measures the velocity spread of the ionized gas. Therefore, the M_*–$\sigma_{H\alpha}$ relation is not directly representative of the relation between stellar mass and SFR.

We explore the existence of a similar correlation between the stellar mass and Δv_{90}. We have stellar mass measurements for seven GRB hosts with Δv_{90} measurements. The right-hand panel in Fig. 1 shows these seven galaxies. Despite the small sample size, we can clearly see a trend of increasing stellar mass with increasing Δv_{90}. The two plots in Fig. 1 show that the velocity widths, measured
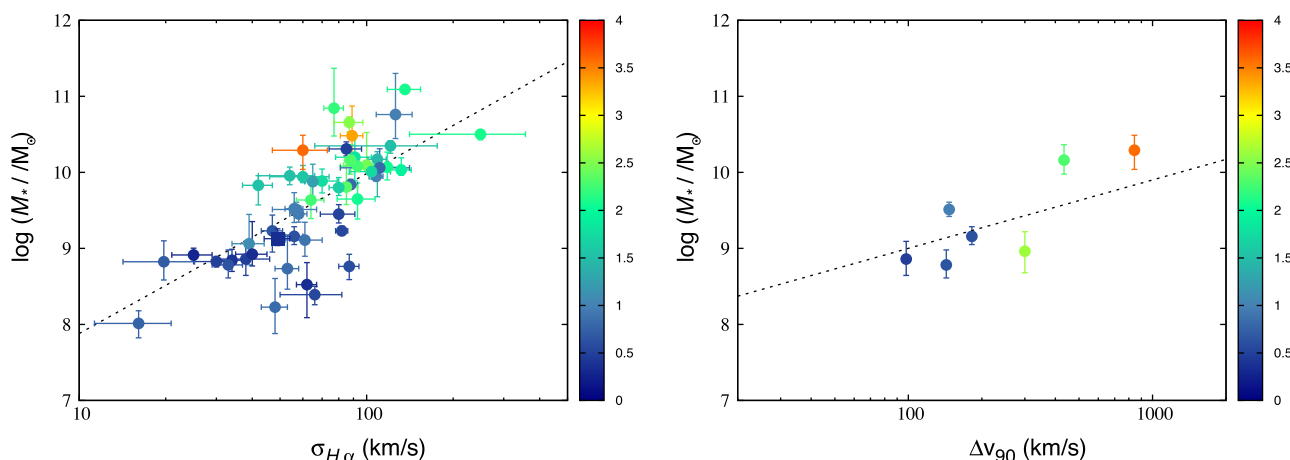

Figure 1. Left-hand panel: stellar mass versus velocity width of bright emission lines, $\sigma_{H\alpha}$, for 52 GRB host galaxies that sample a redshift range from $z = 0.28$ to 3.58. The host galaxy of the ultralong GRB 111209A is marked with a square. Right-hand panel: stellar mass versus velocity width of low-ion absorption lines, Δv_{90}, for seven GRB host galaxies in our sample. The colour bars indicate the redshifts of the GRB hosts in both panels. The dotted lines show the best-fitting lines obtained from the combination of data points in both plots and in Fig. 2 (see Section 3 for details).
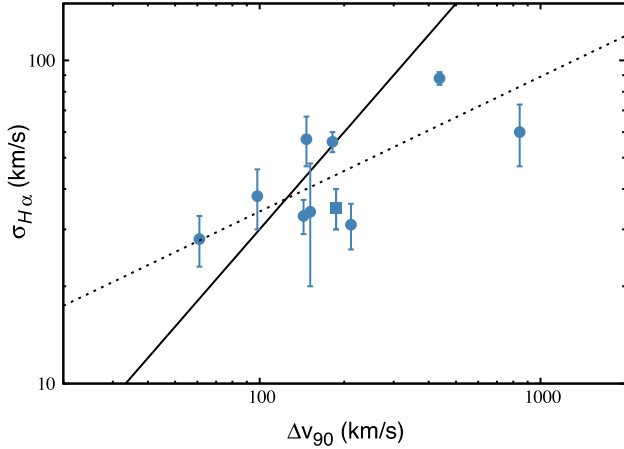
Figure 2. The velocity width of low-ion absorption lines, Δv_{90}, versus the velocity width of bright emission lines, $\sigma_{H\alpha}$, for 10 GRB host galaxies. The dotted line shows the best-fitting line when fitted together with the data presented in Fig. 1 (see Section 3 for details). The solid line ($\Delta v_{90} = 3.29\,\sigma_{H\alpha}$) shows the relation between the two velocities if the absorption and emission profiles were identical. Note that the definition of the two velocity widths is different from each other: $\sigma_{H\alpha}$ is the standard deviation of the fitted Gaussian function to the emission line while Δv_{90} is the velocity interval that contains 90 per cent of the area under the apparent optical depth. Hence, if the emission and absorption profiles were identical, the two velocity widths would not be identical but relate to each other as $\Delta v_{90} = 3.29\sigma_{H\alpha}$. The host galaxy of the ultralong GRB 111209A is marked with a square.

from both absorption and emission methods, can be used as proxies for stellar mass.

The relation between the velocity widths and stellar mass points to a correlation between the two velocity widths. We look for the existence of such a correlation directly using the 10 host galaxies for which we have velocity width measurements in both emission and absorption ($\sigma_{H\alpha}$ and Δv_{90}, respectively). Fig. 2 shows the 10 GRB host galaxies in the Δv_{90}–$\sigma_{H\alpha}$ plane. As expected, we see a trend for an existing correlation between the two velocity widths (keeping in mind the small sample size).

The three aforementioned relations, M_*–$\sigma_{H\alpha}$, M_*–Δv_{90} and $\sigma_{H\alpha}$–Δv_{90}, are not independent from each other. In order to quantitatively study these relations, we use the combination of all data points presented in Figs 1 and 2, and obtain the correlation parameters for the three relations simultaneously. This also allows us to have more reliable results for M_*–Δv_{90} and $\sigma_{H\alpha}$–Δv_{90} relations where the sample sizes are small. We present our method of finding the best-fitting correlation parameters using the combined data points in Appendix A. We find the two velocity widths (in km s^{-1} unit) to relate to stellar mass (in M$_\odot$ unit) as below:

$$M_* = 10^{5.8\pm0.4} \times \sigma_{H\alpha}^{2.1\pm0.2}, \tag{3}$$

$$M_* = 10^{7.2\pm0.7} \times \Delta v_{90}^{0.9\pm0.3}, \tag{4}$$

with an intrinsic scatter of 0.4 and 0.3 dex in stellar mass for the two relations, respectively. And consistently, the two velocity widths follow the relation

$$\sigma_{H\alpha} \propto \Delta v_{90}^{0.4\pm0.2}, \tag{5}$$

with an intrinsic scatter of 0.1 dex on $\sigma_{H\alpha}$. The best-fitting correlations are shown as dotted lines in Figs 1 and 2. Note that the definition of the two velocity widths that we use is different from

each other. The emission velocity width, $\sigma_{H\alpha}$, is the standard deviation of the fitted Gaussian function to the emission line. But Δv_{90} is the velocity interval that contains 90 per cent of the area under the apparent optical depth. For a Gaussian with a standard deviation of σ the 90 per cent area is between -1.645σ and $+1.645\sigma$. Hence if the emission line profiles and the apparent optical depth of the absorption profiles were identical, the two velocity widths should relate to each other simply as $\Delta v_{90} = 3.29\sigma_{H\alpha}$ (shown with a solid line in Fig. 2). This would only affect the intercept in the correlation shown in Fig. 2 and would predict a slope of unity. Therefore the shallow slope of the correlation between the two velocity widths (0.4 in equation 5) is not an artefact of using differently defined velocity widths. However, the GRB host with the largest Δv_{90} (host of GRB 090323A) in Fig. 2 is the only point that is clearly inconsistent with the solid line. To check the significance of the obtained correlation, we exclude this host from the sample and repeat the fitting procedure. We do not find a significant change in the results, i.e. the slope of the correlation in Fig. 2 remains well below one.

The notably different powers in equations (3) and (4), or equivalently the shallow slope of the correlation shown in Fig. 2 suggests significantly large Δv_{90} values especially for galaxies with large stellar masses. Δv_{90} values larger than a few hundreds of km s^{-1} must have significant contributions from components other than rotational motion. In the case of the host of GRB 090323A, the Δv_{90} of 843 km s^{-1} is significantly larger than the rotational velocity expected from its stellar mass of $M_* = 10^{10.3}$ M$_\odot$ that is 213 km s^{-1} based on the sTF relation presented in Übler et al. (2017). The situation is similar in the case of GRB 050820A host with a Δv_{90} of 300 km s^{-1} and a stellar mass of $M_* = 10^{8.96}$ M$_\odot$ (presented in the right-hand panel of Fig. 1) where the rotational velocity is expected to be 90 km s^{-1} (based on the sTF relation presented in Übler et al. 2017).

Large contributions from galactic winds can result in such large absorption widths. While rotation and random motions contribute to the broadening of both the emission and absorption profiles, galactic winds appear to primarily affect the width of the absorption profiles. It is suggested that the Hα emission line is insensitive to a large fraction of the outflow mass, while the ISM absorption lines trace the global galactic winds (e.g. Wood et al. 2015). However, the power-law index of 0.9 in equation (4) ($\Delta v_{90} \propto M_*^{1.1}$) suggests larger galactic wind velocities in GRB host galaxies compared to the general star-forming galaxy population (see e.g. Arabsalmani et al. 2017). Several studies, based on both observations and simulation, have shown that in the general population of starforming galaxies the outflow velocity relates to the stellar mass as $v_{out} \propto M_*^{\sim0.2}$ (see e.g. Bordoloi et al. 2014; Karman et al. 2014; Chisholm et al. 2015, for observational study, and Barai et al. 2015, for studies based on simulation). Also, the velocity of the infalling gas is expected to be smaller than the escape velocity and hence it should relate to stellar mass as $v_{infall} \propto M_*^{\lesssim0.3}$. Through simulations Lagos, Lacey & Baugh (2013) show that the outflow velocity increases with the compactness of the star-forming region (see also Heckman et al. 2015). This should be the case in GRB host galaxies as they have high SFR densities (Kelly et al. 2014) compared to the general galaxy population. This is also supported by the presence of compact regions with recent star-forming activity in GRB environments seen in nearby GRB hosts (see e.g. Fynbo et al. 2000, for the host galaxy of GRB 980425, and Thöne et al. 2008, for the host of GRB 060505A), as well as GRBs being coincident with the brightest regions in their host galaxies (Fruchter et al. 2006; Lyman et al. 2017).

Interacting systems and mergers, as with GRB 090323A mentioned above, could also result in large absorption velocity widths. Indeed for the hosts of GRB 090323A and GRB 121024A, the two host galaxies with the largest Δv_{90}, the absorption profiles contain two main components separated by a few hundreds km s^{-1} in velocity space, which could be due to two interacting galaxies (for GRB 090323 see Savaglio et al. 2012, and for GRB 121024A see Friis et al. 2015). In the case of GRB 050820A (mentioned above) Chen (2012) proposed the broad absorption signatures in the afterglow spectra to be due to the occurrence of the GRB in a dwarf satellite of an interacting system. Other evidence of interacting systems in GRB host galaxies have been discussed by Chary, Becklin & Armus (2002), Wainwright, Berger & Penprase (2007), Chen (2012), Arabsalmani et al. (2015b) and Roychowdhury et al. (in preparation).

4 VELOCITY–METALLICITY CORRELATION IN BOTH ABSORPTION AND EMISSION

Previous studies have shown that the velocity width of low-ion absorption lines correlates linearly with the metallicity (inferred from absorption lines) for DLA galaxies in the sightlines of quasars (QSO–DLAs, Ledoux et al. 2006; Prochaska et al. 2008; Møller et al. 2013; Neeleman et al. 2013). Moreover, Møller et al. (2013) found that the velocity–metallicity (VZ) correlation evolves linearly with redshift up to $z = 2.6$ and then remains unchanged for $z > 2.6$. This correlation is proposed to be representative of an MZ relation for this population of high-redshift galaxies. Christensen et al. (2014) confirmed the consistency of the VZ correlation with the MZ relation for a sample of 12 DLA galaxies with measured stellar masses. Stellar mass measurements for DLA systems in sightlines of quasars have proven to be extremely challenging (especially due to the presence of the bright background quasar).

Arabsalmani et al. (2015a) performed the same study for the DLA systems that are intrinsic to GRB host galaxies and concluded that GRB–DLAs not only follow a VZ correlation, but they are also consistent with that of QSO–DLAs (see also Prochaska et al. 2008). They also found the VZ correlation of GRB–DLAs to obey the same redshift evolution as QSO–DLAs. Fig. 3 shows the VZ correlation for 19 GRB hosts (16 of them are presented in Arabsalmani et al. 2015a) with the host metallicities shifted to the corresponding metallicities at $z = 2.6$ using the evolution of the VZ correlation derived by Møller et al. (2013). In order to shift the metallicity of each host to a reference redshift (here $z = 2.6$) we calculate the offset between the measured metallicity and the VZ correlation at the redshift of the host. We then place the host at the same offset from the VZ correlation at the reference redshift (here $z = 2.6$; see Arabsalmani et al. 2015a, for this approach in considering the effect of the redshift evolution). This is only to visualize the correlation after taking the redshift evolution into account. We have here chosen the reference redshift of $z = 2.6$ since beyond this redshift the VZ correlation derived by Møller et al. (2013) does not evolve. But it is all the same if we choose any other reference redshift for presenting the redshift-corrected VZ correlation.

In studying the VZ correlation we are restricted to $z \gtrsim 1.7$ since absorption metallicity measurements for GRB hosts are limited to redshifts above $\sim$1.7 (observations of short-lasting GRBs optical afterglows are usually limited to ground-based telescopes that do not allow the detection of Lyman α lines in the spectra of GRBs at $z \lesssim 1.7$ due to atmospheric cut-off). However, metallicity measurements based on emission methods are available at lower redshifts. This allows us to investigate the relation between the emission
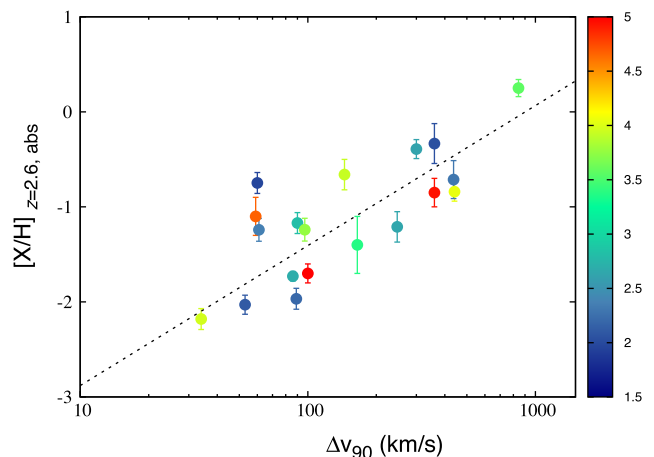

Figure 3. Correlation between absorption metallicity and velocity width of absorption lines, Δv_{90}, for 19 DLA systems intrinsic to GRB host galaxies. The metallicities are corrected for redshift and are set to the corresponding values at $z = 2.6$ (see Section 4 for details). From this redshift onwards the correlation seems to remain unchanged. The colour bar indicates the redshifts of the GRB hosts.

metallicity measurements and the kinematics characteristics of gas in GRB host galaxies at lower redshifts.

Krühler et al. (2015) performed a detailed study of the correlation between emission metallicity measurement and the broadening of the bright emission lines for GRB host galaxies. Splitting their host sample into three redshift bins ($z < 1$, $1 < z < 2$ and $z > 2$) they report a correlation in the two lowest redshift bins, and with essentially no redshift evolution. In the higher redshift bin they find no evidence for a correlation, instead they find strong evidence for an evolution of the intercept (lower panel of their fig. 20).

We further investigate this correlation and its redshift evolution by shifting the metallicity measurements of all the hosts to a fixed redshift. We use the same sample as in Krühler et al. (2015), i.e. 43 GRB hosts with emission metallicity and velocity width measurements, which span a redshift range between $z = 0.28$ and 3.36. First, we use the same approach explained for Fig. 3 and shift all the metallicities to the same reference redshift of $z = 2.6$ using the evolution of the VZ correlation in absorption. The results are shown in the upper panel of Fig. 4. The full sample clearly obeys a tight correlation with an intrinsic scatter of 0.16 dex. This is based on the assumption that metallicities in absorption and emission follow the same redshift evolution that may not be the case. In order to have an independent analysis from absorption studies, we also apply a redshift evolution of the emission-line metallicities of the general population of star-forming galaxies. We adopt the MZ relation and its evolution up to redshift $z = 3.4$ from Maiolino et al. (2008) and Troncoso et al. (2014). For each GRB host, we calculate the offset between the measured metallicity and the MZ relation at the relevant redshift. Using the calculated offsets, we shift all the metallicities to the same reference redshift of $z = 2.6$. This can only be done for those hosts with measured stellar masses, i.e. 33 hosts out of the 43, as the metallicity evolution of the MZ relation is stellar mass dependent. Our results, presented in the lower panel of Fig. 4, show a clear tight correlation for all the 33 GRB hosts. We find the correlation to be (with $\sigma_{H\alpha}$ in km s^{-1} unit)

$$[12 + \log(\text{O/H})]_{z=2.6,\text{emi}} = (1.24 \pm 0.19) \log_{10}(\sigma_{H\alpha})$$
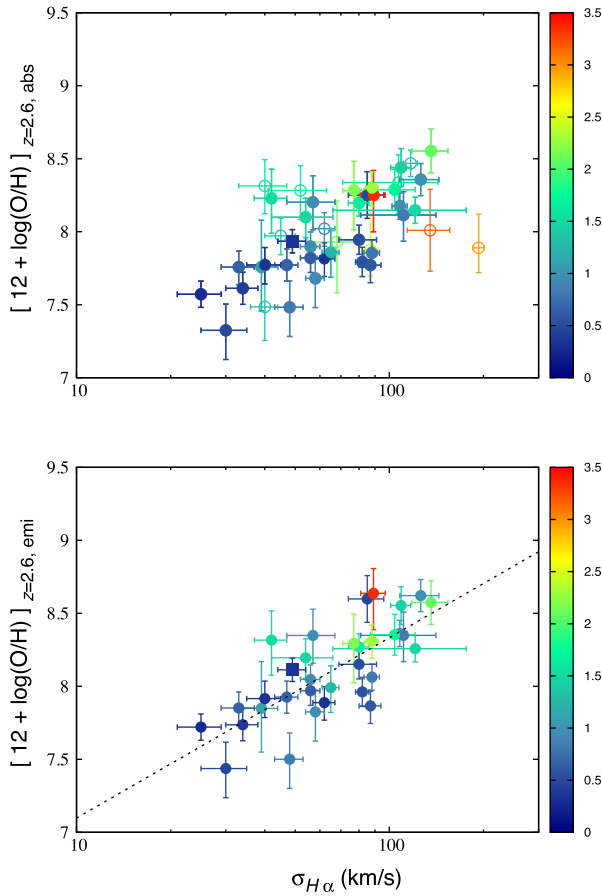$$+ (5.86 \pm 0.35), \quad (6)$$

Figure 4. The correlation between emission metallicity and velocity width of bright emission lines, $\sigma_{H\alpha}$, considering its redshift evolution. The *y*-axis in both panels shows the emission metallicity corrected for redshift evolution that were set to their corresponding values at $z = 2.6$ (see Section 4 for details). In the upper panel the redshift correction of metallicities is based on the redshift evolution of absorption metallicities (derived for QSO–DLAs by Møller et al. 2013 and discussed for GRB–DLAs by Arabsalmani et al. 2015a). In the lower panel the redshift corrections are based on the redshift evolution of emission metallicities obtained for general population of star-forming galaxies (Maiolino et al. 2008). In the upper panel the open circles show those GRB hosts in our sample for which we do not have stellar mass measurements. We do not show these GRB hosts in the lower panel since redshift correction of metallicity measurements following the emission method requires the stellar mass measurements. In the lower panel the dotted line shows the best-fitting correlation line. The colour bar indicates the redshifts of the GRB hosts. The host galaxy of the ultralong GRB 130925A is marked with a square.

with an intrinsic scatter of 0.13 dex. When using either method of applying the redshift correction, the intrinsic scatter of the correlation is comparable with the average uncertainty in the metallicity measurements. This shows that the VZ correlation in emission is a significantly tight correlation. Note that the VZ correlation in absorption has an intrinsic scatter of 0.4 dex that is an about three times larger than the intrinsic scatter of the correlation between $\sigma_{H\alpha}$ and emission metallicity.

For an unbiased comparison of the absorption- versus emission-based redshift evolution we must compare the scatter determined from the two methods using the same sample. Applying the absorption-based evolution to only the GRB hosts with known stellar masses (those shown in the lower panel) we find the intrinsic scatter to be 0.12 dex, somewhat smaller than the scatter in the lower

panel. The emission-based redshift evolution from Maiolino et al. (2008) is determined up to $z \sim 3.5$, while the absorption-based redshift evolution from Møller et al. (2013) is determined back to a redshift of 5.1 and is based on galaxies sampling the entire galaxy luminosity function evenly over a wide range (see fig. 10 in Krogager et al. 2017). The two evolution functions agree well at $z < 2.6$, but at higher redshifts they diverge. The GRB host sample shown in the lower panel of Fig. 4 contains only one host at $z > 2.6$ and hence applying the two evolution functions result in similar scatters on the correlation.

5 MASS–METALLICITY RELATION

The MZ relation is a fundamental scaling relation that provides valuable insights into the processes that take place in formation and evolution of galaxies (Tremonti et al. 2004; Erb et al. 2006; Maiolino et al. 2008; Mannucci et al. 2009; Zahid, Kewley & Bresolin 2011; Troncoso et al. 2014). GRB host galaxies with accurate metallicity measurements obtained via absorption profiles can in principle provide unique tools for studying the MZ relation at high redshifts (see Laskar, Berger & Chary 2011, for the MZ relation at $3 < z < 5$ using GRB hosts). As a subset of star-forming galaxies, GRB hosts are expected to follow the MZ relation of the general star-forming galaxy population. However, several studies have found GRB hosts to fall below the MZ relation towards lower metallicities (Stanek et al. 2006; Kewley et al. 2007; Han et al. 2010; Levesque et al. 2010; Mannucci et al. 2011; Graham & Fruchter 2013; Vergani et al. 2017). The typically low metallicity of GRB host galaxies should in principle put them on the lower mass end of the MZ relation of the general star-forming galaxy population, but still on the MZ relation. Mannucci et al. (2011) suggested that the apparent low metallicity of GRB hosts compared to the general population with similar stellar masses is a consequence of the higher than average SFRs of GRB host galaxies. This was contradicted by Graham & Fruchter (2013) who found that the low-metallicity preference of GRB hosts was not driven by the anticorrelation between star formation and metallicity.

The existence of a MZ relation for GRB hosts and its consistency with the MZ relation of star-forming galaxies has been a subject under debate. Here we use the 33 GRB host galaxies in our sample with measured emission-line metallicities and stellar masses to study the MZ relation for GRB host galaxies. With these 33 GRB hosts we span a redshift range between $z \sim 0.3$ and ~ 3.4 and also cover a stellar mass range of $10^{8.2}$–$10^{11.1} \, M_\odot$. Note that the emission-line metallicity measurements for these 33 GRB hosts, taken from Krühler et al. (2015), are based on the same diagnostics as used in Maiolino et al. (2008) and Troncoso et al. (2014). This is important since we take the MZ relation from these two references for comparison with the GRB host sample. Also, the stellar mass measurements of Krühler & Schady (2017) are obtained using the same methods and assumptions (SED fitting with galaxy templates based on Bruzual & Charlot 2003, assuming exponentially declining star formation histories with the dust attenuation curve from Calzetti et al. 2000) applied for stellar mass measurements in Maiolino et al. (2008) and Troncoso et al. (2014). The only difference is in the assumed IMF: Salpeter IMF used in Maiolino et al. (2008) versus Chabrier IMF used in Krühler et al. (2015). We use a factor of 1.7 (0.23 dex in stellar mass) in order to convert the results based on the Salpeter IMF to the corresponding results based on Chabrier IMF (as done also in Troncoso et al. 2014). Therefore, all the studies presented in this paper are based on assuming a Chabrier IMF.
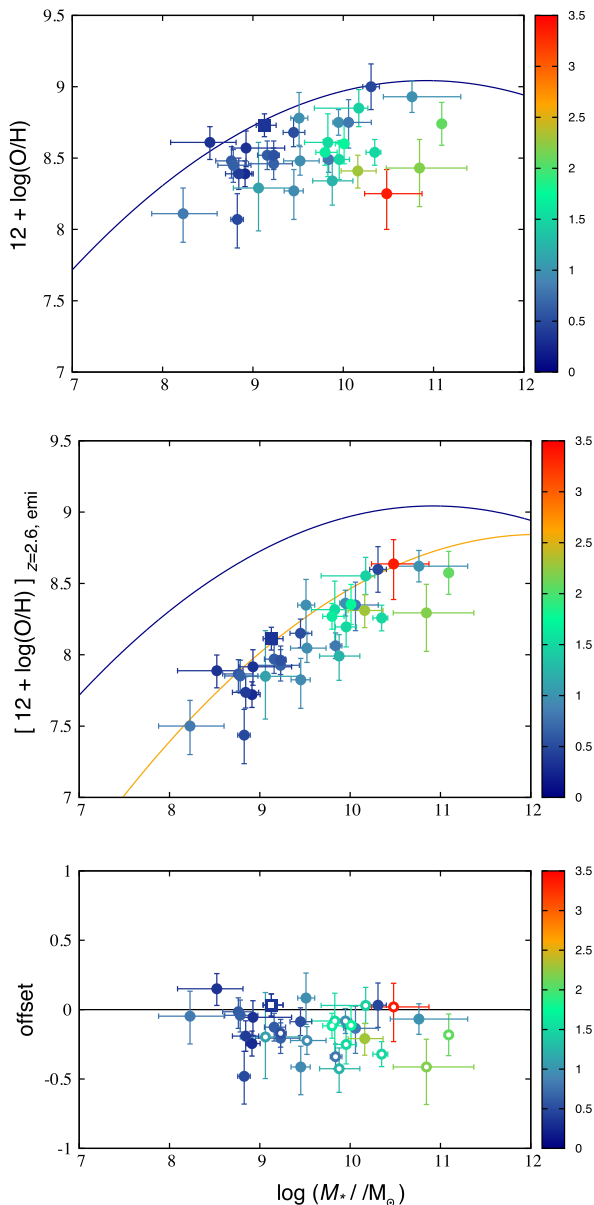
Figure 5. The MZ relation for 33 GRB hosts. *y*-axis shows the measured emission metallicity in the upper panel and its value when shifted to the reference redshift $z = 2.6$ in the middle panel. The solid lines show the MZ relation at $z = 0$ and 2.6 from Maiolino et al. (2008) and Troncoso et al. (2014). The host galaxy of the ultralong GRB 130925A is marked with a square. Lower panel shows the offsets between the metallicity measurements of GRB hosts and the MZ relation. The open circles (and the open square in the case of GRB 130925A) in the lower panel mark the hosts of dust-obscured/dark GRBs. The colour bar indicates the redshifts of the GRBs and the lines.

The upper panel in Fig. 5 shows our GRB host sample compared to the MZ relation of the general star-forming galaxy population (Tremonti et al. 2004; Maiolino et al. 2008). At first glance, the GRB hosts clearly appear to fall well below the MZ relation at $z = 0$. But as expected, GRB hosts with higher redshifts have larger deviations from the local MZ relation. In order to check the consistency of GRB hosts with the evolving MZ relation it is appropriate to do the comparison in a given redshift bin and check if all the galaxies in that bin match the MZ relation at that redshift. But since the small

number of the GRB sample do not allow such a comparison, we instead plot our sample hosts with their metallicities shifted to a reference redshift in the MZ plane and compare them with the MZ relation at a reference redshift. As explained in previous section, for each GRB host we calculate the offset between the GRB host and the MZ relation at the GRB redshift (see the lower panel of Fig. 5). In order to visualize the effect of the redshift evolution and to ease the comparison we place all the GRB hosts in the MZ plane with the quantified offsets from the MZ relation at a reference redshift. The value of this reference redshift has no effect on the results. In order to be consistent with our analysis presented in Section 4, we choose the reference redshift of 2.6.

The middle panel of Fig. 5 shows our GRB host sample with metallicities set at $z = 2.6$. In this plot the GRB hosts appear to track the MZ relation but with an offset towards lower metallicities. The lower panel of Fig. 5 shows the offsets between the GRB hosts and the MZ relation. We find the average offset to be -0.15 ± 0.15 dex. This is in a general agreement with the previous studies finding GRB host galaxies below the MZ relation of the general population. But the offset between GRB host galaxies and the MZ relation is relatively small (see also Japelj et al. 2016), in contradiction with several studies that find GRB host galaxies to fall far below the MZ relation (e.g. Han et al. 2010; Levesque et al. 2010; Graham & Fruchter 2013; Vergani et al. 2017). We find the offset to be comparable with the scatter on the MZ relation of the general population. Also, the average error bar on metallicity measurements for our GRB sample is 0.134 ± 0.002 dex that is comparable with the offset values of 0.148 dex. Therefore it is hard to decide whether this offset is due to systematic effects or the nature of GRB host galaxies. The intrinsic properties of GRB host galaxies such as higher specific star formation rates and star formation densities (e.g. Kelly et al. 2014; Perley et al. 2015) could lead to a similar trend in the MZ plane. It is known that at fixed stellar masses, nearby galaxies with higher gas fractions typically possess lower oxygen abundances (Hughes et al. 2013). So possible higher gas fractions in GRB hosts (consistent with large N(H I) values measured from the Lyman α lines in GRB afterglows) could cause an offset towards lower metallicities. If GRB host galaxies indeed have larger outflows (see Section 3), they would also tend to show lower metallicities compared to the field galaxies with similar stellar masses. Systematic effects in metallicity and stellar mass measurements on the other hand could partially be responsible for the trend of finding GRB hosts with an offset compared to the field galaxies on the MZ plane.

The effects from observational biases (that could result in finding fewer GRBs in dustier environments) can be addressed through the host galaxies of dust-obscured/dark GRBs. Such biases may result in finding more GRBs in galaxies with low to intermediate stellar masses (dustier galaxies tend to have higher stellar masses). This should place the GRB hosts at the lower mass end of the MZ relation, but is not expected to affect the position of the GRB-selected galaxies with respect to the MZ relation. In order to check the significance of such biases in our results, we consider the dust-obscured/dark GRBs in our sample (based on Greiner et al. 2011; Perley et al. 2013, 2016a; Krühler et al. 2015) separately and check whether they show a different trend on the MZ plane compared to the whole sample. In the lower panel of Fig. 5 dust-obscured/dark GRB hosts are marked with the open circles. As expected, there is no clear difference between the dust-obscured/dark hosts and the full sample on the MZ plane. We in fact find that the average offset of the dust-obscured/dark GRB hosts from the MZ relation is -0.18 ± 0.14 dex, consistent with the average offset of our full

sample hosts towards lower metallicities (-0.15 ± 0.15 dex). This confirms that including dust-obscured/dark GRBs in our sample does not affect the scaling relations of the GRB hosts, but instead allows us to have better statistics and to sample larger ranges of galaxy properties that are critical in studying the scaling relations. Also note that the host galaxies of the two ultralong GRBs (GRB 111209A and GRB 130425) appear to fallow the scaling relations of the GRB host sample (see Figs 1, 2, 4 and 5).

In the most recent study, Vergani et al. (2017) use a sample of 21 GRB host galaxies at $z < 2$. At low stellar masses ($M_* < 10^{9.5}\,\mathrm{M_\odot}$) they report an agreement between GRB hosts and the MZ relation (with a similar sample to that of Japelj et al. 2016, and similar conclusions), but they find GRB hosts with $M_* > 10^{10.0}\,\mathrm{M_\odot}$ to be considerably offset from the MZ relation. In order to explore the source of the discrepancy in between our results and the findings of Vergani et al. (2017), we cross-check our sample with their six GRB hosts with $M_* > 10^{10.0}\,\mathrm{M_\odot}$. Three of these hosts are included in our analysis of the MZ relation. For the other three we do not have emission-line metallicity measurements from Krühler et al. (2015) (see Section 2), but the stellar masses are reported for two of them by Krühler & Schady (2017). It appears that for all the five hosts the stellar masses used in Vergani et al. (2017) are systematically larger (by in average 0.53 dex) than the values that we have from Krühler & Schady (2017). This can indeed be the cause behind the discrepancy in between the results. We also notice that at lower masses their sample is dominated by GRB hosts at $z < 1$ where they use stellar masses measured from the same method as in Krühler & Schady (2017); unlike their $z > 1$ sample where stellar masses are measured from the 3.6 μm flux. Hence, at $M_* < 10^{9.5}\,\mathrm{M_\odot}$ their stellar masses are consistent with the measurements used in this paper and so their results are consistent with our findings.

The consistency of the GRB hosts with the MZ relation of the general population encourages the use of GRB-selected galaxies (with their available accurate metallicity measurements) for studying the MZ relation and its evolution at high redshifts ($z \gtrsim 3$). In fact Laskar et al. (2011) used the GRB hosts at $z \sim 3$–5 and found evidence for the existence of the MZ relation and its continued evolution at $z \sim 3$–5. However, it should be noted that the metallicity measurements of GRB hosts at high redshifts are obtained through absorption-line methods which may differ from the emission-line metallicity measurements (see the following section).

6 METALLICITY IN ABSORPTION VERSUS EMISSION

It is necessary to confirm the consistency of the absorption metallicities with metallicity measurements obtained from emission methods before using them to investigate the MZ relation at high redshifts (see Friis et al. 2015, for comparing emission and absorption metallicity measurements in the sole GRB host galaxy with both measurements, Pettini et al. 2002, for a similar study of a Lyman-break galaxy and Noterdaeme et al. 2012; Péroux et al. 2012; Fynbo et al. 2013; Krogager et al. 2013, for similar studies of QSO–DLAs).

It is not clear if the metallicity measurements from absorption and emission methods should be identical as the methods of measuring the two metallicities are completely different. In emission, ratios of strong emission lines (like the ratio of oxygen from forbidden [O II] or [O III] lines to hydrogen obtained from H α or H β lines) are used to derive an oxygen abundance, $12 + \log(\mathrm{O/H})$, as a measure of the metal content. These methods require certain calibrations for strong-line diagnostics that are typically based on the physical conditions present in low-redshift galaxies (for detailed discussions see
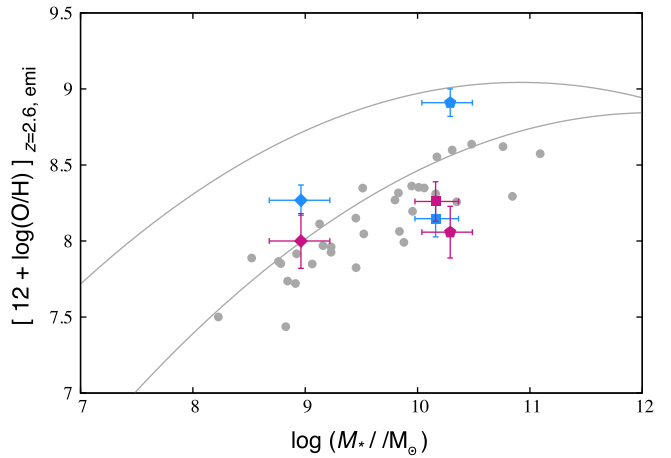

Figure 6. Three GRB hosts with measured stellar mass and absorption metallicity on the MZ plane. The blue points show the three GRB hosts when the emission metallicities are assumed to be identical to absorption metallicity measurements and the magenta points show them with their emission metallicities inferred form scaling relations. GRB 121024A is marked with squares, GRB 090323A with hexagons and GRB 050820A with diamonds. The grey circles show the GRB host sample with measured emission metallicities and stellar masses. The solid lines present the MZ relation of the general star-forming galaxy population at $z = 0$ and 2.6.

Maiolino et al. 2008; Steidel et al. 2014). In absorption the ratio of the column densities of metals (obtained from metal lines) to that of neutral hydrogen (obtained from Lyman α line) provides a direct and accurate metallicity measurement; unlike in emission where various metallicity calibrations give rise to metallicities that differ by up to 0.8 dex for the same galaxies (Kewley & Ellison 2008), absorption metallicities do not suffer from calibration uncertainties and therefore are more reliable measurements of metal enrichment, especially at high redshifts (keeping in mind that absorption profiles provide information only in a narrow beam along the GRB sightline). In addition, the emission and absorption profiles used in the two methods trace different phases of gas and different regions of the galaxy. The absorption methods probe the metal enrichment of gas extended to the outer most regions of the galaxy. On the other hand, the metallicity obtained from emission methods measures the metal enrichment of the ionized gas in the star-forming regions of the galaxy, where star formation activities have enriched the metal content of the gas. Therefore it is not unexpected if the metallicity measurements from the two methods are different.

In order to investigate the effect of the metallicity measurement methods in studying the MZ relation we use the three GRB host galaxies in our sample for which we have both absorption metallicity and stellar mass measurements. These are the hosts of GRB 050820A at $z = 2.61$, GRB 090323A at $z = 3.58$ and GRB 121024A at $z = 2.30$. The host galaxy of GRB 121024A is the sole host with measurements for both absorption and emission metallicities. The two metallicity measurements for this galaxy are consistent with each other (Friis et al. 2015). First, we assume that the emission metallicities are identical with the metallicity measurements determined from absorption lines. The blue points in Fig. 6 show the three hosts in the MZ plane assuming that the emission and absorption metallicities are identical. All metallicities are set to be at $z = 2.6$. Next, we infer an emission metallicity for each of these hosts from their velocity width measurements and the scaling relations discussed in Sections 3 and 4 (the magenta points in

Fig. 6). We can especially justify this approach when inferring an emission metallicity based on the measurements of $\sigma_{H\alpha}$ considering the tightness of the VZ correlation in emission (see Section 4 for details). GRB 121024A host galaxy has a $\sigma_{H\alpha}$ of $88 \pm 4\,\mathrm{km\,s^{-1}}$. Using equation (6) (see the lower panel in Fig. 2), this leads to an inferred emission metallicity of 8.26 ± 0.13 (which includes the intrinsic scatter of the used correlation, 0.13 dex, added in quadrature to the measurement error). Note that our inferred emission metallicity is consistent with the measured value of 8.4 ± 0.4 reported by Friis et al. (2015) and $8.41^{+0.11}_{0.12}$ reported by Krühler et al. (2015) for this GRB host. Similarly, we infer an emission metallicity of 8.04 ± 0.16 for GRB 090323A host with $\sigma_{H\alpha} = 60 \pm 13\,\mathrm{km\,s^{-1}}$. For the host galaxy of GRB 050820A, we use the $\Delta v_{90} = 300\,\mathrm{km\,s^{-1}}$ measurement and infer an emission metallicity of 7.97 ± 0.18. The three hosts with these inferred emission metallicities are presented as magenta circles in Fig. 6. While acknowledging the very small statistics, the inferred emission metallicities appear to better follow the GRB host sample on the MZ plane compared to when the absorption metallicities are assumed to be identical to the emission metallicities. Also, in the host of GRB 090323A, the difference between the two values is significant. But of course, direct measurements of emission metallicity for a handful number of GRB hosts with measured absorption metallicities are required to draw robust conclusions on the relation between metallicity measurements from the two methods.

7 SUMMARY

GRB host galaxies provide a unique opportunity to simultaneously study galaxy properties obtained from absorption and emission methods. This includes metallicity and kinematics characteristics of gas, and their relations with stellar mass, which provides invaluable information on galactic structure and the physical processes leading to their formation and evolution. In this paper we investigate the scaling relations between gas kinematics, metallicity and stellar mass for a large sample of GRB host galaxies, using both absorption and emission methods.

We show that the velocity widths of both absorption and emission lines can be used as a proxy of stellar mass, i.e. all the components contributing to the velocity widths must be controlled by the gravitational potential in the galaxy. We propose that the large values of Δv_{90} ($\Delta v_{90} >$ a few hundreds of $\mathrm{km\,s^{-1}}$) can have significant contributions from galactic winds. Indeed, if galactic winds dominate the velocity widths of ISM absorption lines, they appear to have larger velocities in GRB host galaxies compared to the general star-forming galaxy population with similar stellar masses (see e.g. Arabsalmani et al. 2017). This could be a result of the high SFR densities in GRB hosts. Interacting systems too could be behind such large velocity widths. The possible connection between mergers and GRB events them has been previously pointed out in several cases (Chary et al. 2002; Chen 2012; Arabsalmani et al. 2015b; Roychowdhury et al., in preparation).

We investigate the redshift evolution of the correlation between metallicity and velocity width in emission. By considering redshift evolution, our full GRB host sample (in a redshift range between 0.28 and 3.36) falls on a tight VZ correlation with an intrinsic scatter of 0.13 dex, comparable to the uncertainty of the metallicity measurements. We find the VZ correlation in emission to be significantly tighter compared to that in absorption.

We study the MZ relation of GRB host galaxies using 33 GRB hosts spanning a redshift range between $z \sim 0.3$ and ~ 3.4 and a stellar mass range of $10^{8.2}$–$10^{11.1}\,\mathrm{M_\odot}$. By considering the redshift

evolution of the MZ relation, we find GRB hosts to track the MZ relation of the general star-forming galaxy population with an average offset of 0.15 ± 0.15 dex below the MZ relation. This offset is comparable to the scatter of the MZ relation and also to the average error bars on metallicity measurements of the host sample. It is not clear if this offset is due to the systematic effects or the intrinsic properties of GRB hosts such as high gas fractions and large amounts of outflowing gas.

We investigate the possibility of using absorption-line metallicity measurements of GRB hosts to study the MZ relation at high redshifts. Our analysis shows that the metallicity measurements from both methods can significantly differ from each other and assuming identical measurements from the two methods may result in erroneous conclusions. The different metallicity estimates from the two methods could be partly due to the fact that the emission and absorption profiles trace different phases of gas and different regions of the galaxy.

REFERENCES

Arabsalmani M., Møller P., Fynbo J. P. U., Christensen L., Freudling W., Savaglio S., Zafar T., 2015a, MNRAS, 446, 990
Arabsalmani M., Roychowdhury S., Zwaan M. A., Kanekar N., Michałowski M. J., 2015b, MNRAS, 454, L51
Arabsalmani M. et al., 2017, MNRAS, preprint (arXiv:1709.00424)
Arnouts S., Cristiani S., Moscardini L., Matarrese S., Lucchin F., Fontana A., Giallongo E., 1999, MNRAS, 310, 540
Barai P., Monaco P., Murante G., Ragagnin A., Viel M., 2015, MNRAS, 447, 266
Bordoloi R. et al., 2014, ApJ, 794, 130
Bruzual G., Charlot S., 2003, MNRAS, 344, 1000
Calzetti D., Armus L., Bohlin R. C., Kinney A. L., Koornneef J., Storchi-Bergmann T., 2000, ApJ, 533, 682
Castro S., Galama T. J., Harrison F. A., Holtzman J. A., Bloom J. S., Djorgovski S. G., Kulkarni S. R., 2003, ApJ, 586, 128
Castro Cerón J. M., Michałowski M. J., Hjorth J., Malesani D., Gorosabel J., Watson D., Fynbo J. P. U., Morales Calderón M., 2010, ApJ, 721, 1919
Castro-Tirado A. J. et al., 2010, A&A, 517, A61
Chabrier G., 2003, PASP, 115, 763
Chary R., Becklin E. E., Armus L., 2002, ApJ, 566, 229
Chen H.-W., 2012, MNRAS, 419, 3039
Chen H.-W., Prochaska J. X., Bloom J. S., Thompson I. B., 2005, ApJ, 634, L25
Chisholm J., Tremonti C. A., Leitherer C., Chen Y., Wofford A., Lundgren B., 2015, ApJ, 811, 149
Christensen L., Hjorth J., 2017, MNRAS, 470, 2599

Christensen L., Hjorth J., Gorosabel J., 2004, A&A, 425, 913
Christensen L., Møller P., Fynbo J. P. U., Zafar T., 2014, MNRAS, 445, 225
Cucchiara A., Fumagalli M., Rafelski M., Kocevski D., Prochaska J. X., Cooke R. J., Becker G. D., 2015, ApJ, 804, 51
De Cia A. et al., 2011, MNRAS, 412, 2229
D'Elia V. et al., 2010, A&A, 523, A36
D'Elia V., Campana S., Covino S., D'Avanzo P., Piranomonte S., Tagliaferri G., 2011, MNRAS, 418, 680
D'Elia V. et al., 2014, A&A, 564, A38
Dessauges-Zavadsky M., Prochaska J. X., D'Odorico S., Calura F., Matteucci F., 2006, A&A, 445, 93
de Ugarte Postigo A. et al., 2012, A&A, 548, A11
Erb D. K., Shapley A. E., Pettini M., Steidel C. C., Reddy N. A., Adelberger K. L., 2006, ApJ, 644, 813
Friis M. et al., 2015, MNRAS, 451, 167
Fruchter A. S. et al., 2006, Nature, 441, 463
Fumagalli M. et al., 2012, ApJ, 757, L22
Fynbo J. U. et al., 2000, ApJ, 542, L89
Fynbo J. P. U. et al., 2006, A&A, 451, L47
Fynbo J. P. U., Prochaska J. X., Sommer-Larsen J., Dessauges-Zavadsky M., Møller P., 2008, ApJ, 683, 321
Fynbo J. P. U. et al., 2009, ApJS, 185, 526
Fynbo J. P. U. et al., 2013, MNRAS, 436, 361
Glazebrook K., 2013, Publ. Astron. Soc. Aust., 30, e056
Graham J. F., Fruchter A. S., 2013, ApJ, 774, 119
Greiner J. et al., 2011, in McEnery J. E., Racusin J. L., Gehrels N., eds, AIP Conf. Proc. Vol. 1358, Gamma Ray Bursts 2010. Am. Inst. Phys., New York, p. 121
Greiner J. et al., 2015, ApJ, 809, 76
Han X. H., Hammer F., Liang Y. C., Flores H., Rodrigues M., Hou J. L., Wei J. Y., 2010, A&A, 514, A24
Hartoog O. E. et al., 2015, A&A, 580, A139
Heckman T. M., Alexandroff R. M., Borthakur S., Overzier R., Leitherer C., 2015, ApJ, 809, 147
Hughes T. M., Cortese L., Boselli A., Gavazzi G., Davies J. I., 2013, A&A, 550, A115
Ilbert O. et al., 2006, A&A, 457, 841
Jakobsson P. et al., 2004, A&A, 427, 785
Jakobsson P. et al., 2006, A&A, 460, L13
Japelj J. et al., 2016, A&A, 590, A129
Karman W., Caputi K. I., Trager S. C., Almaini O., Cirasuolo M., 2014, A&A, 565, A5
Kassin S. A. et al., 2007, ApJ, 660, L35
Kelly P. L., Filippenko A. V., Modjaz M., Kocevski D., 2014, ApJ, 789, 23
Kennicutt R. C., Evans N. J., 2012, ARA&A, 50, 531
Kewley L. J., Ellison S. L., 2008, ApJ, 681, 1183
Kewley L. J., Brown W. R., Geller M. J., Kenyon S. J., Kurtz M. J., 2007, AJ, 133, 882
Krogager J.-K. et al., 2013, MNRAS, 433, 3091
Krogager J.-K., Møller P., Fynbo J. P. U., Noterdaeme P., 2017, MNRAS, 469, 2959
Krühler T., Schady P., 2017, 10.6084/m9.figshare.4776886.v2
Krühler T. et al., 2012, A&A, 546, A8
Krühler T. et al., 2013, A&A, 557, A18
Krühler T. et al., 2015, A&A, 581, A125
Lagos C. d. P., Lacey C. G., Baugh C. M., 2013, MNRAS, 436, 1787
Laskar T., Berger E., Chary R.-R., 2011, ApJ, 739, 1
Ledoux C., Petitjean P., Fynbo J. P. U., Møller P., Srianand R., 2006, A&A, 457, 71
Ledoux C., Vreeswijk P. M., Smette A., Fox A. J., Petitjean P., Ellison S. L., Fynbo J. P. U., Savaglio S., 2009, A&A, 506, 661
Le Floc'h E. et al., 2003, A&A, 400, 499
Levan A. J. et al., 2014, ApJ, 781, 13
Levesque E. M., Berger E., Kewley L. J., Bagley M. M., 2010, AJ, 139, 694
Lyman J. D. et al., 2017, MNRAS, 467, 1795
Maiolino R. et al., 2008, A&A, 488, 463
Mannucci F. et al., 2009, MNRAS, 398, 1915

Mannucci F., Salvaterra R., Campisi M. A., 2011, MNRAS, 414, 1263
Miller S. H., Bundy K., Sullivan M., Ellis R. S., Treu T., 2011, ApJ, 741, 115
Modjaz M. et al., 2008, AJ, 135, 1136
Møller P., Fynbo J. P. U., Ledoux C., Nilsson K. K., 2013, MNRAS, 430, 2680
Nagao T., Maiolino R., Marconi A., 2006, A&A, 459, 85
Neeleman M., Wolfe A. M., Prochaska J. X., Rafelski M., 2013, ApJ, 769, 54
Noterdaeme P. et al., 2012, A&A, 540, A63
Nuza S. E., Tissera P. B., Pellizza L. J., Lambas D. G., Scannapieco C., de Rossi M. E., 2007, MNRAS, 375, 665
Perley D. A. et al., 2013, ApJ, 778, 128
Perley D. A. et al., 2015, ApJ, 801, 102
Perley D. A. et al., 2016a, ApJ, 817, 7
Perley D. A. et al., 2016b, ApJ, 817, 8
Péroux C., Bouché N., Kulkarni V. P., York D. G., Vladilo G., 2012, MNRAS, 419, 3060
Pettini M., Kellogg M., Steidel C. C., Dickinson M., Adelberger K. L., Giavalisco M., 1998, ApJ, 508, 539
Pettini M., Shapley A. E., Steidel C. C., Cuby J.-G., Dickinson M., Moorwood A. F. M., Adelberger K. L., Giavalisco M., 2001, ApJ, 554, 981
Pettini M., Rix S. A., Steidel C. C., Adelberger K. L., Hunt M. P., Shapley A. E., 2002, ApJ, 569, 742
Price P. A. et al., 2007, ApJ, 663, L57
Prochaska J. X., Wolfe A. M., 1998, ApJ, 507, 113
Prochaska J. X., Chen H.-W., Wolfe A. M., Dessauges-Zavadsky M., Bloom J. S., 2008, ApJ, 672, 59
Puech M. et al., 2008, A&A, 484, 173
Puech M., Hammer F., Flores H., Delgado-Serrano R., Rodrigues M., Yang Y., 2010, A&A, 510, A68
Salvaterra R. et al., 2009, Nature, 461, 1258
Savaglio S., 2006, New J. Phys., 8, 195
Savaglio S., Glazebrook K., Le Borgne D., 2006, in Holt S. S., Gehrels N., Nousek J. A., eds, AIP Conf. Proc. Vol. 836, Gamma-Ray Bursts in the Swift Era. Am. Inst. Phys., New York, p. 540
Savaglio S., Glazebrook K., Le Borgne D., 2009, ApJ, 691, 182
Savaglio S. et al., 2012, MNRAS, 420, 627
Schady P. et al., 2015, A&A, 579, A126
Schulze S. et al., 2015, ApJ, 808, 73
Simard L., Pritchet C. J., 1998, ApJ, 505, 96
Sokolov V. V. et al., 2001, A&A, 372, 438
Sparre M. et al., 2014, ApJ, 785, 150
Stanek K. Z. et al., 2006, Acta Astron., 56, 333
Steidel C. C. et al., 2014, ApJ, 795, 165
Tanvir N. R. et al., 2009, Nature, 461, 1254
Thöne C. C. et al., 2008, ApJ, 676, 1151
Thöne C. C. et al., 2013, MNRAS, 428, 3590
Tremonti C. A. et al., 2004, ApJ, 613, 898
Troncoso P. et al., 2014, A&A, 563, A58
Tully R. B., Fisher J. R., 1977, A&A, 54, 661
Übler H. et al., 2017, ApJ, 842, 121
Vergani S. D. et al., 2015, A&A, 581, A102
Vergani S. D. et al., 2017, A&A, 599, A120
Vernet J. et al., 2011, A&A, 536, A105
Vogt N. P., Forbes D. A., Phillips A. C., Gronwall C., Faber S. M., Illingworth G. D., Koo D. C., 1996, ApJ, 465, L15
Vreeswijk P. M. et al., 2004, A&A, 419, 927
Wainwright C., Berger E., Penprase B. E., 2007, ApJ, 657, 367
Warren S. J., Møller P., Fall S. M., Jakobsen P., 2001, MNRAS, 326, 759
Watson D. et al., 2006, ApJ, 652, 1011
Wolf C., Podsiadlowski P., 2007, MNRAS, 375, 1049
Wood C. M., Tremonti C. A., Calzetti D., Leitherer C., Chisholm J., Gallagher J. S., 2015, MNRAS, 452, 2712
Zafar T., Watson D., Fynbo J. P. U., Malesani D., Jakobsson P., de Ugarte Postigo A., 2011, A&A, 532, A143
Zahid H. J., Kewley L. J., Bresolin F., 2011, ApJ, 730, 137

SUPPORTING INFORMATION

Supplementary data are available at *MNRAS* online.

Table 1. GRB host sample (82 GRB hosts).

Please note: Oxford University Press is not responsible for the content or functionality of any supporting materials supplied by the authors. Any queries (other than missing material) should be directed to the corresponding author for the article.

APPENDIX A

A1 Intrinsic scatter of the correlation

Throughout this paper we investigate the scaling relations between the GRB hosts properties in the form of linear correlations. We explain here the method used for obtaining the correlation parameters.

We basically need to find out the linear correlation between the two measurable quantities, y and x, in the form of $y = a + bx$, using a data set containing N data points with measured values of x_i and y_i for the ith point. In some cases, the measurement errors of data points are non-symmetric and a Monte Carlo method should be used to obtain the best-fitting parameters for the correlation. However, investigating the effect of the asymmetry of the error bars, we find it to be ignorable. One reason for this is the negligible asymmetry of the error bars and the other is the dominating effect of the intrinsic scatter of the correlations, σ_{scatter} (discussed below), compared to the measurement error bars. Therefore, we use the standard least-square method, assuming the measurement errors of each point to be the average of the lower and upper measurement errors of that point. But of course we include the intrinsic scatter of the correlation as a free parameter in the χ^2 by adding it up to the measurement error of each point in the quadratic form (see Møller et al. 2013). The χ^2 then will be

$$\chi^2 = \sum_{i=1}^{N} \frac{(a + bx_i - y_i)^2}{\sigma_{y,i}^2 + b^2 \sigma_{x,i}^2 + \sigma_{\text{scatter}}^2}, \tag{A1}$$

where $\sigma_{x,i}$ and $\sigma_{y,i}$ are the average of the lower and upper measurement errors on x_i and y_i, respectively, and a, b and σ_{scatter} are the three free parameters.

A2 The three correlations

The three correlations between M_*, $\sigma_{\text{H}\alpha}$ and Δv_{90} are not independent from each other and hence they get defined by four parameters:

$$M_* = a + b \, \sigma_{\text{H}\alpha},$$
$$M_* = c + d \, \Delta v_{90}. \tag{A2}$$

The two correlations in equation (A2) automatically define the correlation between $\sigma_{\text{H}\alpha}$ and Δv_{90}. In order to find the best fits for the four parameters we use all the three sets of data points: n_i pairs of $(M_*, \sigma_{\text{H}\alpha})$, n_j pairs of $(M_*, \Delta v_{90})$ and n_k pairs of $(\sigma_{\text{H}\alpha} - \Delta v_{90})$. Some of the data points are shared between the three sets. In order to do a χ^2 minimization that takes into account all three correlations and the sharing of data points, we solve a matrix optimization as follows. We write the three correlations for all the data points:

$$a + b \, \sigma_{\text{H}\alpha,i} = M_{*,i},$$

$$c + d \, \Delta v_{90,j} = M_{*,j},$$

$$a + b \, \sigma_{\text{H}\alpha,k} - c - d \, \Delta v_{90,k} = 0, \tag{A3}$$

where $i = 1, \ldots, n_i$, $j = n_i + 1, \ldots, n_i + n_j$ and $k = n_j + 1, \ldots, n_j + n_k$. To solve the equations, we write them as a matrix equation: $\mathbf{A} \cdot \boldsymbol{p} = \boldsymbol{M}$, where $\mathbf{A}$ is the matrix,

$$\begin{bmatrix} 1 & \sigma_{\text{H}\alpha,i} & 0 & 0 \\ 0 & 0 & 1 & \Delta v_{90,k} \\ 1 & \sigma_{\text{H}\alpha,k} & -1 & -\Delta v_{90,k} \end{bmatrix},$$

$\boldsymbol{p}$ is the vector (a, b, c, d) and $\boldsymbol{M}$ is the vector $(M_{*,i}, M_{*,j}, 0 \ldots 0)$ with the last k elements being 0. The dimensions of matrix $\mathbf{A}$, vector $\boldsymbol{p}$ and vector $\boldsymbol{M}$ are $4(i + j + k)$, 4 and $i + j + k$, respectively.

In order to make this a χ^2 optimization, one has to multiply both sides of each equation with the appropriate weights before solving it. The weights are $[\sigma_{M_*,i}^2 + \sigma_{\text{scatter}, M_* - \sigma_{\text{H}\alpha}}^2]^{-0.5}$ for 1 to i, $[\sigma_{M_*,k}^2 + \sigma_{\text{scatter}, M_* - \Delta v_{90}}^2]^{-0.5}$ for n_{i+1} to $n_i + n_j$ and $[(b \sigma_{M_*,k})^2 + \sigma_{\text{scatter}, \sigma_{\text{H}\alpha} - \Delta v_{90}}^2]^{-0.5}$ for n_{j+1} to $n_j + n_k$. With these weights, minimizing $|\mathbf{A} \cdot \boldsymbol{p} - \boldsymbol{M}|^2$ is equivalent to the χ^2 minimization.

If a point appears in two of the data sets, the weights have to be reduced in order to avoid counting that measurement twice. Though we find this not to change our results significantly. Finally, we use NUMPY.LINALG.LSTSQ routine to solve the matrix equation.

A3 An example for Δv_{90} measurement

Here we present an example for the Δv_{90} measurement. The left-hand panel of Fig. A1 shows the Mn II, 2294 absorption profile in the VLT/X-shooter spectrum of GRB 121024A at $z = 2.30$. Friis et al. (2015) present a detailed study of the absorption profiles in this GRB spectrum by modelling the identified profile with a multi (five) Voigt-profile components. The right-hand panel in the figure shows the optical depth corresponding to the Mn II, 2294 line. The dotted lines marked with v_5 and v_{95} indicate the velocities at which 5 and 95 per cent of the total area under the optical depth spectrum are covered, respectively. The shaded area shows the 90 per cent of the area under the apparent optical depth spectrum. Δv_{90} is defined as $v_{95} - v_5$. We measure a Δv_{90} of $434 \, \text{km s}^{-1}$ for this multicomponent system.
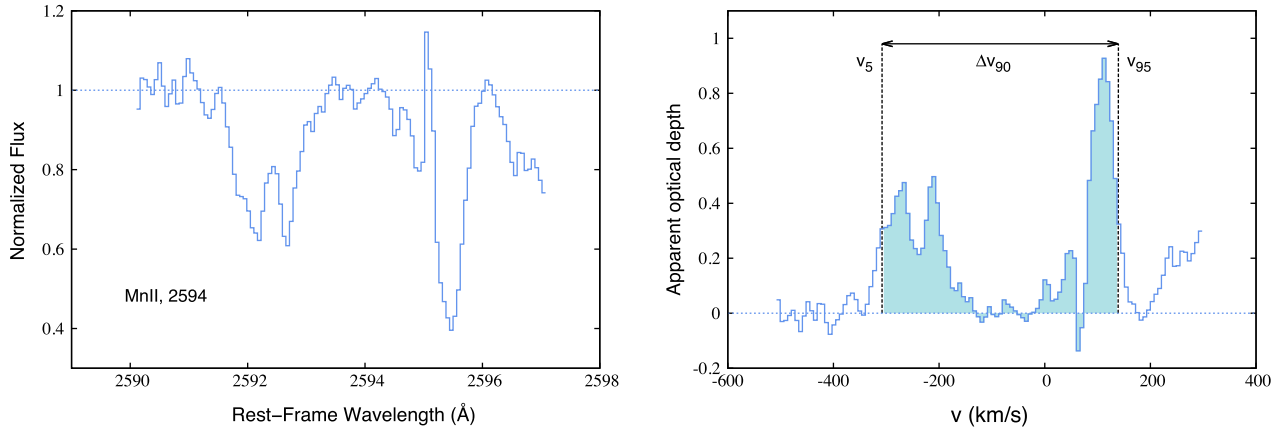
Figure A1. An example for Δv_{90} measurement from an absorption profile. Left-hand panel: the Mn II, 2294 absorption profile in the VLT/X-shooter spectrum of GRB 121024A at $z = 2.30$. Right-hand panel: the optical depth corresponding to the Mn II, 2294 line. The dotted lines marked with v_5 and v_{95} indicate the velocities at which 5 and 95 per cent of the total area under the optical depth spectrum are covered, respectively. The shaded area shows the 90 per cent of the area under the apparent optical depth spectrum. Δv_{90} is defined as $v_{95} - v_5$.

This paper has been typeset from a TEX/LATEX file prepared by the author.